AN ANALYTICAL MODEL FOR THE ACCRETION OF DARK MATTER SUBHALOS

Xiaohu Yang[1], H.J. Mo[2], Youcai Zhang[1,4], Frank C. van den Bosch[3]

Draft version January 19, 2013

ABSTRACT

An analytical model is developed for the mass function of cold dark matter subhalos at the time of accretion and for the distribution of their accretion times. Our model is based on the model of Zhao et al. (2009) for the median assembly histories of dark matter halos, combined with a simple log-normal distribution to describe the scatter in the main-branch mass at a given time for halos of the same final mass. Our model is simple, and can be used to predict the un-evolved subhalo mass function, the mass function of subhalos accreted at a given time, the accretion-time distribution of subhalos of a given initial mass, and the frequency of major mergers as a function of time. We test our model using high-resolution cosmological N-body simulations, and find that our model predictions match the simulation results remarkably well. Finally, we discuss the implications of our model for the evolution of subhalos in their hosts and for the construction of a self-consistent model to link galaxies and dark matter halos at different cosmic times.

Subject headings: cosmology: dark matter halos – galaxies: formation – galaxies: halos

1. INTRODUCTION

In the current Cold Dark Matter (hereafter CDM) paradigm of structure formation, a key concept in the build-up of structure in the universe is the hierarchical formation of dark matter halos. Galaxies and other luminous objects are assumed to form by cooling and condensation of baryons within these halos (see Mo, van den Bosch & White 2010, for an overview). In this scenario, a detailed understanding of the formation and structure of dark matter halos is of fundamental importance for predicting the properties of luminous objects, such as galaxies and clusters of galaxies.

The formation history of a CDM halo is conveniently represented by its merger tree, which describes how its progenitors merge and accrete during its entire formation history. For a given cosmological model, such merger trees can be constructed either from N-body simulations or from Monte-Carlo realizations based on the extended Press-Schechter (PS) formalism (Press & Schechter 1974; Bond et al. 1991; Bower 1991; Lacey & Cole 1993; Sheth, Mo & Torman 2001). In recent years, much effort has been made to characterize and understand the statistical properties of halo formation in a CDM cosmogony. One particular aspect of the halo formation process is the existence of a subhalo population, which is produced by the accretion and survival of progenitors at various times (e.g. Klypin et al. 1999; Moore et al. 1999; Kravtsov et al. 2004; Gao et al. 2004; De Lucia et al. 2004; van den Bosch et al. 2005; Diemand et al. 2007; Giocoli et al. 2008a,b; Springel et al. 2008; Wetzel et al.

2009; Angulo et al. 2009; Li et al. 2009). Since galaxies may form at the centers of these progenitors and merge into the final halo along with their hosts (e.g. Kang et al. 2005), the statistical properties of the subhalo population are expected to be closely linked to those of satellite galaxies. One of the basic properties of the subhalo population is the mass function of the progenitors of subhalos (i.e., the masses of the subhalos at their moment of accretion). Following van den Bosch et al. (2005), we refer to this mass function as the *un-evolved* subhalo mass function, to distinguish it from the *evolved* subhalo mass function that refers to the present day masses of dark matter subhalos (see §3 for details). A number of recent investigations have used these subhalo mass functions in an attempt to characterize the galaxy-dark matter connection across cosmic times (e.g. Vale & Ostriker 2004, 2006; Zheng et al. 2005, 2007; Conroy et al. 2006, 2007; Conroy & Wechsler 2009; Yang et al. 2009, 2011; Li et al. 2009; Moster et al. 2010; Behroozi et al. 2010; Wang & Jing 2010; Wetzel & White 2010; Neistein et al. 2011; Avila-Reese & Firmani 2011).

So far the subhalo mass function has been studied with N-body simulations and Monte-Carlo realizations of the extended PS formalism (e.g. Sheth & Lemson 1999; Somerville & Kolatt 1999; Cole et al. 2000; van den Bosch et al. 2005; Giocoli et al. 2008a; Cole et al. 2008; Parkinson et al. 2008; Fakhouri & Ma 2008; Fakhouri et al. 2010). In this paper we show that a simple analytical model can be constructed to describe not only the mass distribution of subhalos but also the distribution of their accretion times. We use N-body simulations to demonstrate that the model is remarkably accurate. The model is not only simple to implement, but also provides important insights into the formation and evolution of dark matter halos and subhalos. Furthermore, as we briefly discuss in §5, our model also provides a self-consistent way to link galaxies and dark matter halos at different redshifts.

The structure of the paper is organized as follows. In Section 2 we outline the simulations based on which we will test our model. In Section 3 we describe our model.

[1] Key Laboratory for Research in Galaxies and Cosmology, Shanghai Astronomical Observatory; the Partner Group of MPA; Nandan Road 80, Shanghai 200030, China; E-mail: xhyang@shao.ac.cn
[2] Department of Astronomy, University of Massachusetts, Amherst MA 01003-9305
[3] Astronomy Department, Yale University, P.O. Box 208101, New Haven, CT 06520-8101
[4] Graduate School of the Chinese Academy of Sciences, 19A, Yuquan Road, Beijing, China

In Section 4 we present our model predictions for the conditional mass function of subhalos, the major merger rates, and the subhalo mass function. These model predictions are tested against N-body simulation results in Section 4. Finally, in Section 5 we discuss the universality of our model for other models of structure formation, and discus how our model can be used to study the evolution of subhalos in their hosts and to construct self-consistent models that link galaxies and dark matter halos across cosmic times.

Throughout this paper, we use 'ln' to denote natural logarithm and 'log' to denote the 10-based logarithm.

2. THE SIMULATIONS

Before presenting our model, let us first describe briefly the the N-body simulations to be used to test the model.

We use two different N-body simulations that assume the same cosmology but use different box sizes (mass resolutions). Both simulations were carried out using the massively parallel GADGET2 code (Springel et al. 2001a, 2005). The simulations evolved 1024^3 dark matter particles in periodic boxes of $100\,h^{-1}$Mpc and $300\,h^{-1}$Mpc on a side, respectively, from redshift $z = 100$ to the present epoch ($z = 0$). The particle masses and softening lengths are, respectively, $6.93 \times 10^7\,h^{-1}\mathrm{M}_\odot$ and $2.25\,h^{-1}$kpc for the $100\,h^{-1}$Mpc box simulation, and $1.87 \times 10^9\,h^{-1}\mathrm{M}_\odot$ and $6.75\,h^{-1}$kpc for the $300\,h^{-1}$Mpc box simulation. The cosmological parameters used in the simulations are based on those published in Dunkley et al. (2009): $\Omega_{\mathrm{m}} = \Omega_{\mathrm{dm}} + \Omega_{\mathrm{b}} = 0.258$, $\Omega_{\mathrm{b}} = 0.044$, $h = 0.719$, $\Omega_\Lambda = 0.742$, $n = 0.963$, and $\sigma_8 = 0.796$. Unless stated otherwise, our model predictions are also for the ΛCDM cosmology with this particular set of parameters. For both simulations, a total of 100 outputs in equal $\log(1 + z)$ interval were made, starting from $z = 50$ (for $300\,h^{-1}$Mpc box) and $z = 20$ (for $100\,h^{-1}$Mpc box) to $z = 0$.

Dark matter halos were identified from the simulations at each output using the standard friends-of-friends (FOF) algorithm (Davis et al. 1985) with a linking length of 0.2 times the mean interparticle separation. Here we keep all halos with at least 20 particles. Based on halos at different outputs, halo merger trees were constructed (see Lacey & Cole 1993). A halo in an earlier output is considered to be a progenitor of the present halo if more than half of its particles are found in the present halo. The main branch of a merger tree is defined to consist of all the progenitors one goes through as one climbs from the bottom to the top, choosing always the most massive branch at every branching point. These progenitors are referred to as the main-branch progenitors, and the time dependence of the main branch mass is referred to as the assembly history. In our analysis based on the $300\,h^{-1}$Mpc box simulation, we randomly choose about 200 trees, from the total merger tree catalogue, to sample each of the two massive bins at $M_h \sim 10^{14.5}\,h^{-1}\mathrm{M}_\odot$ and $M_h \sim 10^{14.0}\,h^{-1}\mathrm{M}_\odot$, and about 2000 trees to sample each of the low-mass bins at $M_h \sim 10^{13.0}\,h^{-1}\mathrm{M}_\odot$ and $M_h \sim 10^{12.0}\,h^{-1}\mathrm{M}_\odot$, with bin widths $\Delta \log M_h \sim 0.7, 0.1, 0.1, 0.02$, respectively. Our tests later are mainly based on the $300\,h^{-1}$Mpc box simulation. However, in many cases we also use halo merger trees obtained from the $100\,h^{-1}$Mpc box simulation to achieve bet-

ter mass resolution. Specifically, about 7, 36, 400 and 2000 trees are selected from this simulation to sample the merger histories for halos with $M_h \sim 10^{14.5}\,h^{-1}\mathrm{M}_\odot$, $\sim 10^{14.0}\,h^{-1}\mathrm{M}_\odot$, $\sim 10^{13.0}\,h^{-1}\mathrm{M}_\odot$ and $\sim 10^{12.0}\,h^{-1}\mathrm{M}_\odot$, with bin widths $\Delta \log M_h \sim 0.5, 0.5, 0.5, 0.3$, respectively.

3. THE MODEL

Now we come back to our modeling of the accretion of subhalos. We want to obtain the distribution of dark matter subhalos with respect to their mass at accretion, m_a, and their accretion redshift, z_a, in a host halo of mass M_0 at redshift z_0. For convenience we use

$$s_a \equiv \sigma_a^2 = \sigma^2(m_a); \qquad S_0 \equiv \sigma_0^2 = \sigma^2(M_0) \qquad (1)$$

to label the masses, m_a and M_0, and

$$\delta_a \equiv \delta_c(z_a); \qquad \delta_0 \equiv \delta_c(z_0) \qquad (2)$$

to label the redshifts z_a and z_0. Here $\sigma(M)$ is the variance of the linear density field at $z = 0$ on mass scale M, and $\delta_c(z) \approx 1.686/D(z)$ [with $D(z)$ the linear grow factor normalized to unity at $z = 0$] is the critical density of spherical collapse at redshift z. We write the mean number of subhalos of mass m_a accreted at redshift z_a in a host halo (M_0, δ_0) as

$$\mathrm{d}^2 N_a = \mathcal{N}_a(s_a, \delta_a | S_0, \delta_0)\mathrm{d}\ln m_a\,\mathrm{d}\ln(1 + z_a)\,. \qquad (3)$$

The mean mass, $\overline{M}(z)$, of the main branch halos for all (M_0, δ_0) - halos is in general a monotonically decreasing function of redshift (e.g., Avila-Reese et al. 1998; van den Bosch et al. 2002; Wechsler et al. 2002), and we write $\overline{M}_a \equiv \overline{M}(z_a)$. Hence, for given (M_0, δ_0) we can use $\overline{M}_a$ as a time-variable. Denote by $\mathcal{F}(s_a, \delta_a | S_0, \delta_0; \overline{M}_a)$ the mean fraction of the total mass accreted in the 'time-interval' $[\overline{M}_a - \mathrm{d}\overline{M}_a, \overline{M}_a]$ that is in halos of mass m_a. We can write

$$\mathrm{d}^2 N_a = \frac{1}{m_a}\mathcal{F}(s_a, \delta_a | S_0, \delta_0; \overline{M}_a)\mathrm{d}\overline{M}_a\,\mathrm{d}s_a\,. \qquad (4)$$

It then follows that

$$\mathcal{N}_a = \mathcal{F}(s_a, \delta_a | S_0, \delta_0; \overline{M}_a)\frac{\mathrm{d}s_a}{\mathrm{d}m_a}\frac{\mathrm{d}\overline{M}_a}{\mathrm{d}\ln\delta_a}\frac{\mathrm{d}\ln\delta_a}{\mathrm{d}\ln(1 + z_a)}\,. \qquad (5)$$

Note that $\mathrm{d}s_a/\mathrm{d}m_a$ is determined by the perturbation power spectrum, $\mathrm{d}\ln\delta_a/\mathrm{d}\ln(1 + z_a)$ by the linear growth factor, and $\mathrm{d}\overline{M}(z_a)/\mathrm{d}\ln\delta_a$ by the mean halo assembly history.

We can integrate $\mathcal{N}_a$ over the mean mass assembly history to obtain the so-called un-evolved subhalo mass function:

$$\frac{\mathrm{d}N_a}{\mathrm{d}\ln m_a} = \int \mathcal{N}_a(s_a, \delta_a | S_0, \delta_0)\mathrm{d}\ln(1 + z_a)$$

$$= \int_{m_a}^{M_0} \mathcal{F}(s_a, \delta_a | S_0, \delta_0; \overline{M}_a)\frac{\mathrm{d}s_a}{\mathrm{d}m_a}\mathrm{d}\overline{M}_a\,. \qquad (6)$$

This function describes the distribution of the masses at accretion of all subhalos accreted into the main-branch of the merger history of the (M_0, δ_0) host halo. Thus for a given cosmology, one can obtain both $\mathcal{N}_a$ and the un-evolved subhalo mass function once models for $\mathcal{F}(s_a, \delta_a | S_0, \delta_0; \overline{M}_a)$ and for the mean halo assembly history are adopted. In general $\mathcal{F}$ can be obtained using

halo merger trees constructed either from numerical simulations or from analytical models, such as the extended PS formalism. Here we develop a simple analytical model based on the statistical properties of halo assembly histories, instead of on the full merger trees.

Consider a halo whose main-branch mass is M_a at z_a. Since we are modeling the accretion of subhalos into the main branch of its merger tree, we must have that $m_a \leq m_{\max}$ with[5]

$$m_{\max} \equiv \text{MIN}(M_a, M_0/2) \,. \qquad (7)$$

Thus, a simple model for the mass fraction in (m_a, δ_a)-progenitors to be accreted at z_a may be written as

$$\Phi(s_a, \delta_a | S_0, \delta_0; M_a)$$
$$= \begin{cases} B^{-1} F(s_a, \delta_a | S_0, \delta_0; M_a) & \text{if } m_a \leq m_{\max} \\ 0 & \text{otherwise} \,, \end{cases} \qquad (8)$$

where $F(s_a, \delta_a | S_0, \delta_0; M_a)$ is the mass fraction in progenitor halos of mass m_a to be accreted at redshift z_a. The normalization factor,

$$B = \int_{S(m_{\max})}^{\infty} F(s_a, \delta_a | S_0, \delta_0; M_a) \mathrm{d}s_a \,, \qquad (9)$$

is the total mass fraction of all progenitors that can be accreted into the main branch. Now suppose that the distribution of M_a at z_a is given by $P(M_a | S_0, \delta_0)$ then

$$\mathcal{F}(s_a, \delta_a | S_0, \delta_0; \overline{M}_a)$$
$$= \int \Phi(s_a, \delta_a | S_0, \delta_0; M_a) P(M_a | S_0, \delta_0) \mathrm{d}M_a \,. \qquad (10)$$

3.1. Models for $F(s_a, \delta_a | S_0, \delta_0; M_a)$

Model I: According to the extended PS formalism, the fraction of mass of halo (M_1, z_1) that is in progenitor halos of mass M_2 at redshift $z_2 > z_1$ can be written as

$$f(S_2, \delta_2 | S_1, \delta_1) = \frac{1}{\sqrt{2\pi}} \frac{\delta_2 - \delta_1}{(S_2 - S_1)^{3/2}} \exp\left[-\frac{(\delta_2 - \delta_1)^2}{2(S_2 - S_1)} \right] \qquad (11)$$

(see Lacey & Cole 1993). Thus, the simplest model is to assume $F(s_a, \delta_a | S_0, \delta_0; M_a) = f(s_a, \delta_a | S_0, \delta_0)$. However, $f(s_a, \delta_a | S_0, \delta_0)$ is the mean for all (S_0, δ_0)-halos, and so such an assumption completely ignores the scatter in the assembly history, i.e. the dependence on M_a. A better approximation is to assume that $F(s_a, \delta_a | S_0, \delta_0; M_a)$ is independent of S_0 and δ_0, i.e. the accretion properties at z_a is determined entirely by the mass of the main-branch halo at that redshift regardless of where the halo will end up at $z = 0$. In this case, we may write

$$F(s_a, \delta_a | S_0, \delta_0; M_a) \, \mathrm{d}\ln\delta_a$$
$$= f[s_a, \delta_a + \mathrm{d}\delta_a | S(M_a), \delta_a]$$
$$= \frac{1}{\sqrt{2\pi}} \frac{\mathrm{d}\delta_a}{[s_a - S(M_a)]^{3/2}} \,, \qquad (12)$$

where the extended PS formula (11) is used in the second equation. In what follows we will refer this model as

---

[5] Note that m_a reflects the mass of the progenitor halo which, after accretion into the main-branch, increases the main-branch mass to M_a

Model I. Note that as we will illustrate in section 4.1, this model does not match well with the simulation results.

Model II: Numerical simulations have shown that the PS formula (11) is not accurate. Attempts have been made to come up with better approximations (e.g. Sheth & Tormen 2004; Neistein & Dekel 2008; Cole et al. 2008; Parkinson et al. 2008). According to the empirical modification proposed by Parkinson et al. (2008), we may write

$$F(s_a, \delta_a | S_0, \delta_0; M_a) \, \mathrm{d}\ln\delta_a$$
$$= \frac{1}{\sqrt{2\pi}} \frac{\mathrm{d}\delta_a}{[s_a - S(M_a)]^{3/2}} G\left[\frac{\sigma_a}{\sigma(M_a)}, \frac{\delta_a}{\sigma(M_a)} \right] \,, \qquad (13)$$

where $G(x, y) = G_0 x^{\gamma_1} y^{\gamma_2}$, with $G_0 = 0.57$, $\gamma_1 = 0.38$ and $\gamma_2 = -0.01$. This model will be referred to as Model II in what follows.

Model III: Other than the above two models, we find by trial and error that the following simple modification of the extended PS formula provides a much more **accurate** model for F:

$$F(s_a, \delta_a | S_0, \delta_0; M_a) \, \mathrm{d}\ln\delta_a$$
$$= \frac{1}{\sqrt{2\pi}} \frac{\delta_a - \delta_M}{(s_a - S_M)^{3/2}} \exp\left[-\frac{(\delta_a - \delta_M)^2}{2(s_a - S_M)} \right] \,, \qquad (14)$$

where δ_M corresponds to the redshift at which the main branch has the mass

$$M_{\max} = \text{MIN}(\mathcal{M}_a + m_{\max}, M_0) \,, \qquad (15)$$

with $\mathcal{M}_a$ the *median* main-branch mass (not to be confused with the *mean* branch mass $\overline{M}_a$) and

$$S_M \equiv \sigma_M^2 = \sigma^2(M_{\max}) \,. \qquad (16)$$

This model will be referred to as Model III.

3.2. Halo Assembly History

Following Zhao et al. (2009), the median accretion rate of a (M_0, δ_0) host halo at redshift z can be written as

$$\frac{\mathrm{d}\ln\sigma(M)}{\mathrm{d}\ln\delta_c(z)} = \frac{1}{5.85} \left\{ w[\delta_c(z), \sigma(M)] - p[\delta_c(z); \delta_0, \sigma_0] \right\} \,. \qquad (17)$$

Here

$$w = \frac{\delta_c(z)}{\sigma(M)} 10^{-\mathrm{d}\ln\sigma(M)/\mathrm{d}\ln M} \,; \qquad (18)$$

and

$$p[\delta_c(z); \delta_0, \sigma_0] \qquad (19)$$
$$= p(\delta_0; \delta_0, \sigma_0) \times \text{Max}\left[0, 1 - \frac{\log\delta_c(z) - \log\delta_0}{0.272/w(\delta_0, \sigma_0)} \right] \,,$$

with

$$p(\delta_0; \delta_0, \sigma_0) = \frac{1}{1 + [w(\delta_0, \sigma_0)/4]^6} \frac{w(\delta_0, \sigma_0)}{2} \,. \qquad (20)$$

One can obtain the median main-branch mass $\mathcal{M}_a(z_a | M_0, z_0)$ by simply integrating Eq. (17) from redshift z_0 to z_a. The solid curves in Fig. 1 correspond to the median assembly histories thus obtained for four different host halo masses, as indicated in each panel. For comparison, the thin, jagged curves correspond to
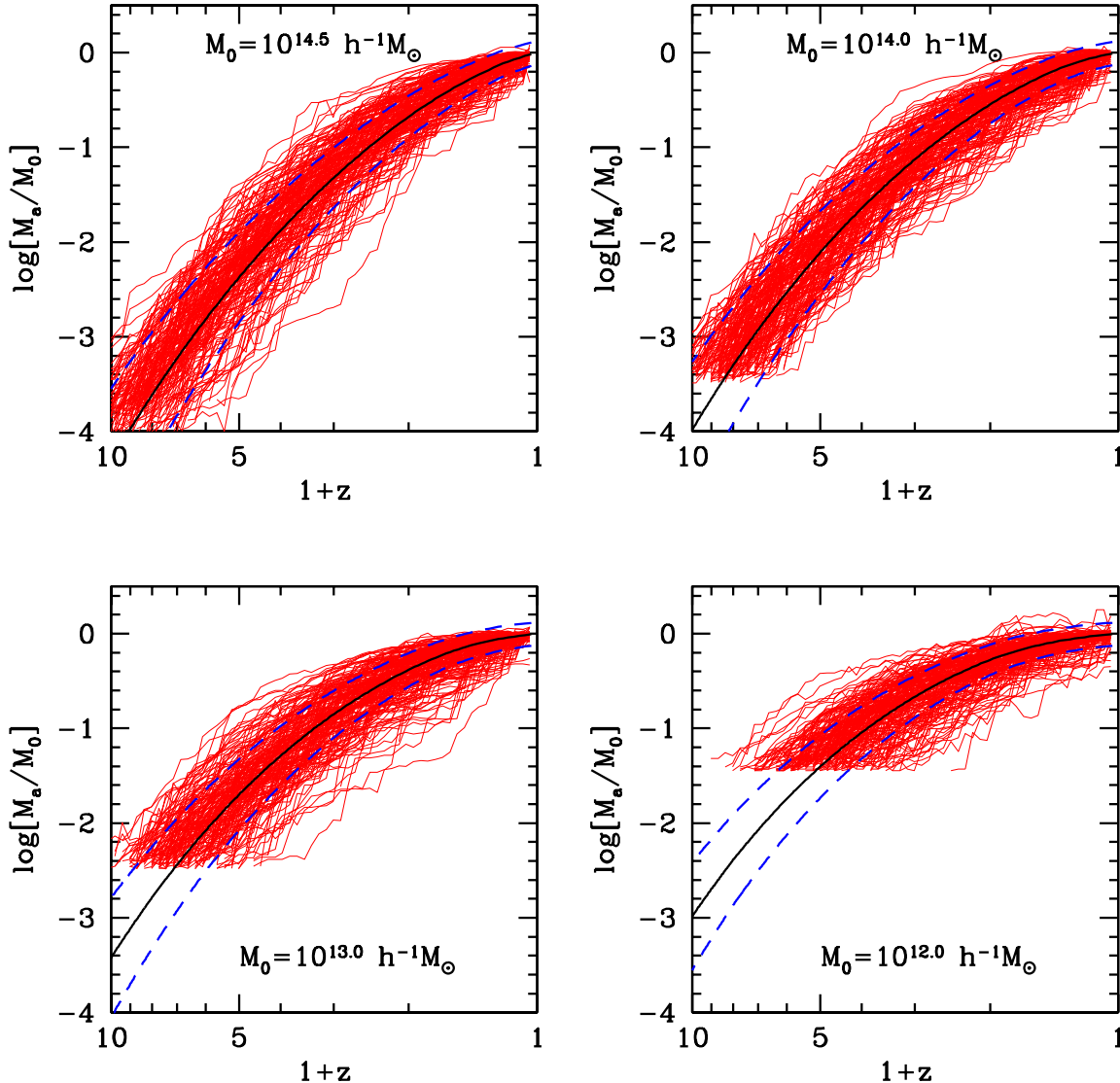
FIG. 1.— The thin solid curves in each panel are the assembly histories of 200 simulated halos of a given final mass as indicated in the panel. The solid curve is the predicted median assembly history by the Zhao et al. (2009) model. The two dashed curves are the $\pm 1\sigma$-range given by equation (21).

mass accretion histories obtained from N-body simulations. The results are shown for a selection of 200 main branch assembly histories for halos in each mass bin extracted from the $300h^{-1}$Mpc box simulation. Clearly, the model of Zhao et al. (2009) yields *median* mass assembly histories that are in excellent agreement with simulation results.

In order to proceed we need to make one important addition. The Zhao et al. (2009) model only gives the median assembly history. However, a complete model for the un-evolved subhalo distribution with respect to the mass at accretion and the redshift of accretion requires the full distribution function $P(M_a|S_0,\delta_0)$. It is easy to understand that the dispersion in M_a plays an important role. Since by definition the masses of subhalos are all smaller than that of the main progenitor, using the mean assembly history would imply that at any given time no accreted subhalo can have a mass larger than the mean mass on the main branch. Clearly, when allowing for dispersion in the main-branch masses, this

constraint is no longer present. The different panels of Fig. 2 show the distributions of the main-branch halo masses at different redshifts obtained from simulations (histograms). Results are shown for halos with redshift zero masses $\sim 10^{14.5}\ h^{-1}$M$_\odot$ (panels in the upper two rows) and $\sim 10^{13.0}h^{-1}$M$_\odot$ (panels in the lower two rows), respectively. All the distributions are reasonably well described by a log-normal distribution, with median given by the Zhao et al. (2009) model, and with a dispersion (in 10-based logarithm) given by

$$\sigma = 0.12 - 0.15 \log(\mathcal{M}_a/M_0), \qquad (21)$$

as shown by the solid curves in the figure. The lack of low-mass main-branch progenitors in the simulation apparent in the bottom right two panels is simply due to the mass limit in the N-body simulation. For comparison, the dashed lines in Fig. 1 show the $\pm 1\sigma$ range given by Eq. (21), together with the median given by the Zhao et al. (2009) model (solid curves).
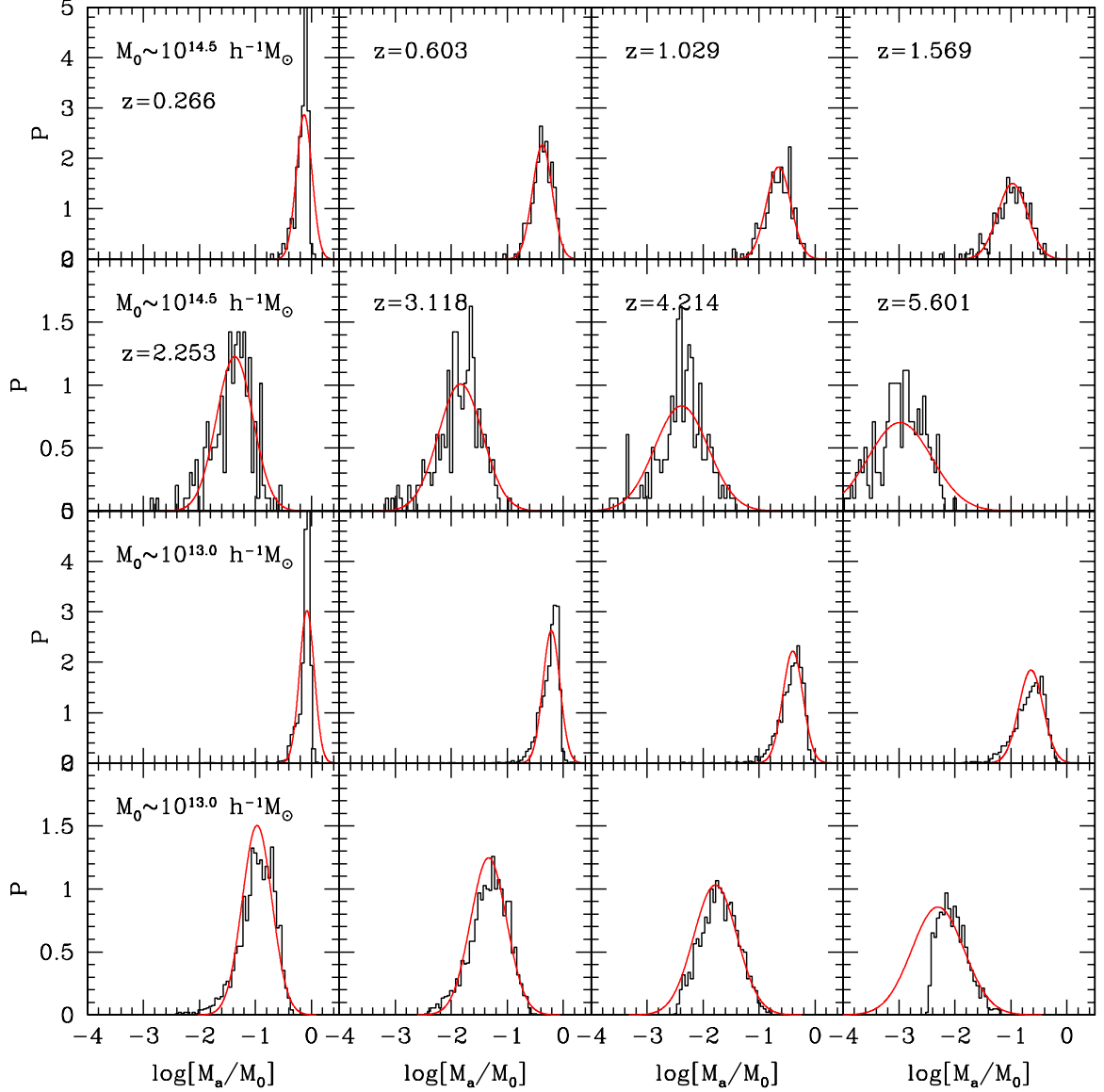
An important advantage of the log-normal form for

FIG. 2.— The distribution of the main-branch mass at different redshifts obtained from N-body simulations (histograms). Results are shown for halos with final masses $\sim 10^{14.5}$ $h^{-1}\mathrm{M}_\odot$ (upper two rows) and $\sim 10^{13.0}$ $h^{-1}\mathrm{M}_\odot$ (lower two rows), respectively. The smooth curves are the log-normal model described in Section 3.2.

the distribution $P(M_a|S_0, \delta_0)$ is that it is straightforward to compute the *average* accretion rate $\mathrm{d}\overline{M}_a/\mathrm{d}\ln(1 + z_a)$ (see Eq. [5]). After all, for a log-normal distribution the average $\overline{M}_a$ is related to the median $\mathcal{M}_a$ according to $\overline{M}_a = e^{(\ln(10)\sigma)^2/2} \mathcal{M}_a$. Thus, assuming a log-normal distribution, we can simply use the Zhao et al. (2009) model for the *median* assembly history to obtain the *mean* accretion rate. Fig. 3 shows the mass accretion rate $\mathrm{d}(\overline{M}_a/M_0)/\mathrm{d}\log(1 + z)$ for halos with different final masses. The dashed curve in each panel is the prediction of the Zhao et al. (2009) model of the median together with the log-normal distribution described above.

In the simulations, especially for small halos at low redshifts, there are time-steps over which the accretion rate is negative. This can come about due to, for instance, tidal stripping by neighboring structures, the loss of unbound subhalos or unbound particles, the fragmentation

of halos, and the FOF-bridging problem. The Zhao et al. (2009) model has taken such effects explicitly into account via a correction factor in equation (19). In general, however, it is possible to have two different definitions of the un-evolved subhalo population, one based on all subhalos that have entered the main branch at some point (but are not necessarily bound to or located within the final halo), and the other based on those that have more than half of their particles ending up in the final halo. In this paper we adopt the first definition in which the accretion rate is determined by all subhalos that have been accreted onto the main branch at some point in time, regardless of whether they have left the main branch again or not. The open circles in Fig. 3 show the simulation results based on this definition. As one can see, the mean mass accretion rates predicted by the Zhao et al. (2009) model match well the simulation results over a large range of redshift; the mismatch seen
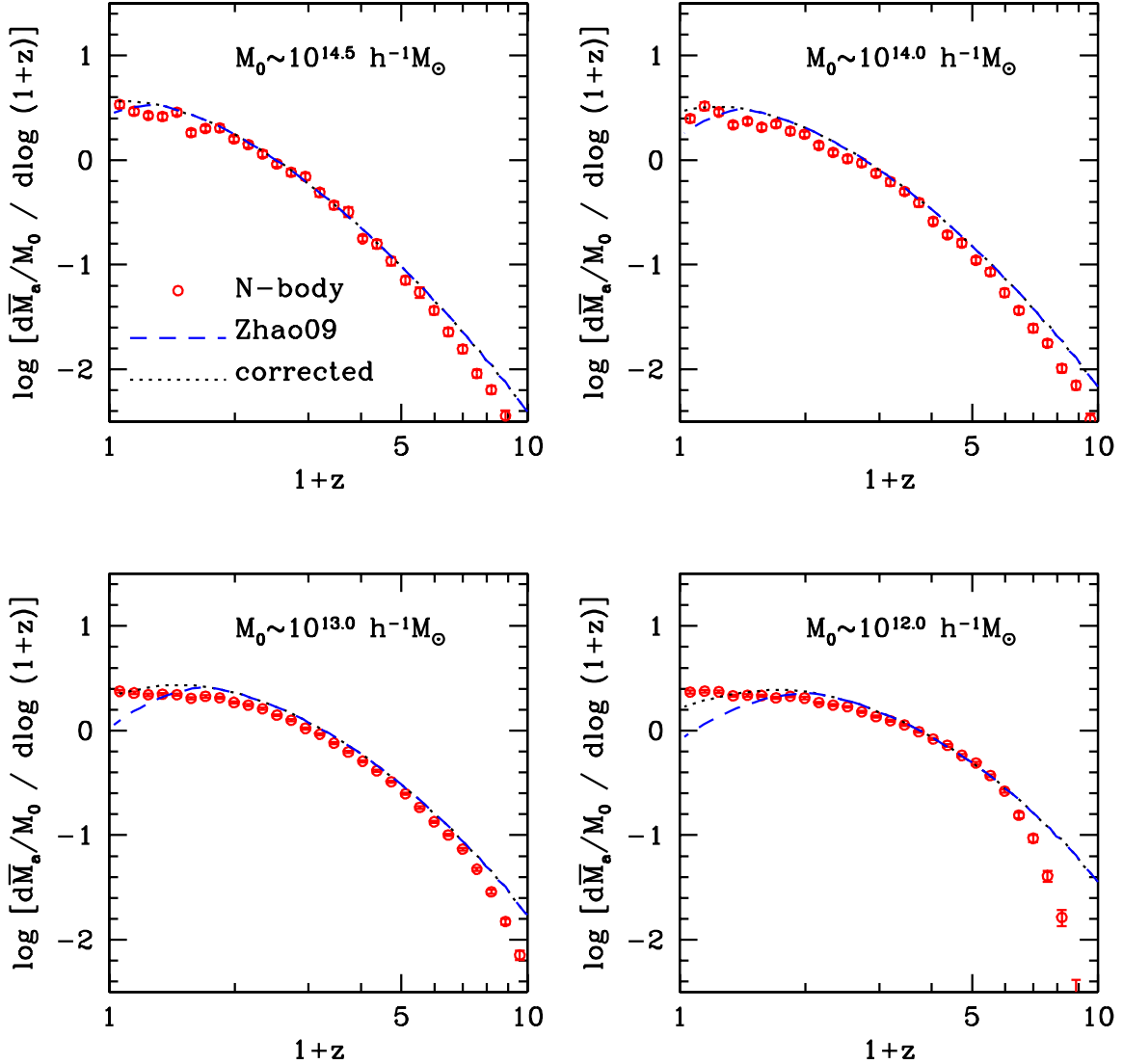
FIG. 3.— The mean mass accretion rate of host halos with different final masses. The open circles in each panel show the rate in terms of $d\log(1+z)$ obtained from N-body simulations, normalized by the mass of the host halo, with error-bars obtained from 200 bootstrap resampling of the host halos. The dashed line is the model prediction of Zhao et al. (2009), while the dotted line shows the corrected mass accretion rate according to equation (22).

at high-z for low-mass halos is simply an artefact due to the limited numerical resolution of the simulation. The only significant discrepancy occurs for low-mass halos at low redshift where the predicted rate is lower than the simulated rate. This discrepancy is mainly due to the fact that the Zhao et al. (2009) model tries to account for the affects of tidal stripping and the presence of un-bound subhalos. For our definition of the un-evolved subhalo population, however, such correction is not required when computing $d\overline{M}_a/d\ln(1+z)$. As discussed in Zhao et al. (2009), this can be achieved by simply setting

$$p[\delta_c(z); \delta_0, \sigma_0] = 0 \qquad (22)$$

in Eq. (17). The dotted lines in Fig. 3 show the predictions based on Eq. (22). Clearly this simple modification works remarkably well, bringing the predictions in good agreement with the simulation results.

If one is interested in using the second definition for the population of subhalos, one can still use our model but with Eq. (22) replaced by Eq. (19). In what follows, we present predictions of Model III based on the first definition, corresponding to Eq. (22). We have tested, though, that using the second definition instead yields results that are very similar, except when it concerns the subhalos accreted at low redshifts in low-mass host halos.

4. TEST WITH N-BODY SIMULATIONS

In this section we use the N-body simulations described in Section 2 to test our models for the distribution of subhalos with respect to their accretion redshift and their mass at accretion.

4.1. The conditional mass function

The first quantity we consider is the conditional mass function of subhalos in host halos of different masses (Eq. [10]). From the halo merger trees constructed from the simulations, we measure the mass distribution of accreted subhalos within equal $\log(1+z)$-bins centered at
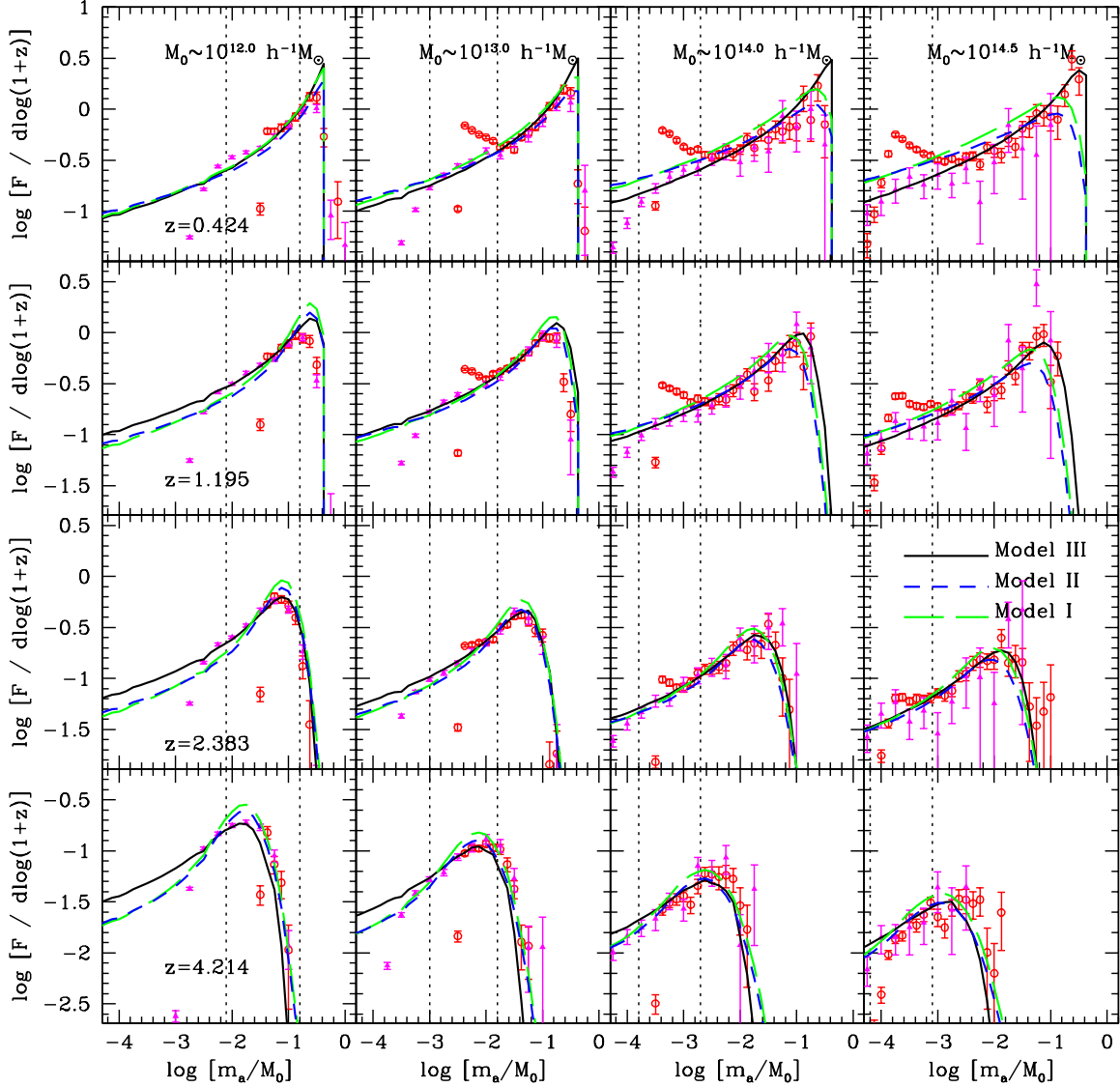
FIG. 4.— The conditional mass distribution of subhalos in host halos of different masses (different columns) at different redshifts (different rows). The symbols are results from N-body simulations, with error-bars obtained from 200 bootstrap resampling of the host halos. In each panel, results are shown for both high- (100 h^{-1}Mpc box; filled triangles) and low- (300 h^{-1}Mpc box; open circles) resolution simulations. In the high-resolution simulation, unbound particles are removed (see text for details). The long-dashed, dashed and solid lines show the predictions of Models I, II, and III respectively. Finally, the vertical dotted lines in each panel correspond to the mass limit of 100 particles in the high- (left line) and low- (right line) resolution simulations, respectively. Note that bin widths in different columns are different.

0.42, 1.2, 2.4 and 4.2, respectively. The results are shown in Fig. 4 as open circles (for $300\,h^{-1}$Mpc simulation box) and filled triangles (for $100\,h^{-1}$Mpc simulation box) where the errorbars have been obtained from 200 bootstrap resamples of the population of host halos. Each column shows results for host halos with a given mass, while each row shows the results at a given redshift. Note that, because of mass resolution and because of tidal effects, a fraction of the subhalos containing $\lesssim 100$ particles, especially those near massive halos, are not gravitationally bound. This is the reason for the artificial upturn in the conditional mass function seen in the low-resolution simulation results at low redshift. In the literature this problem has been treated either by using only halos that contain large enough number of particles or by getting rid of unbound particles from halos. For instance, the SUB-

FIND halo finder developed by Springel et al. (2001b) tries to separate bound and unbound structures in FOF halos. In Benson et al. (2001), unbound particles are removed iteratively from each halo until the total energy of the halo becomes negative. In order to quantify the magnitude of this effect, we have also constructed halo merger trees using a method similar to Benson et al. (2001) to calculate the number of bound particles per (sub)-halo. Halos with less than 20 bound particles are discarded from our sample. In Fig. 4, we show the results obtained from the $100\,h^{-1}$Mpc simulation box in which we removed the halos with bound particles less than 20 (using the method described above), together with the results from the $300\,h^{-1}$Mpc simulation box without such treatment. The dotted, vertical lines correspond to halos with 100 particles in each of the two simulations, and are
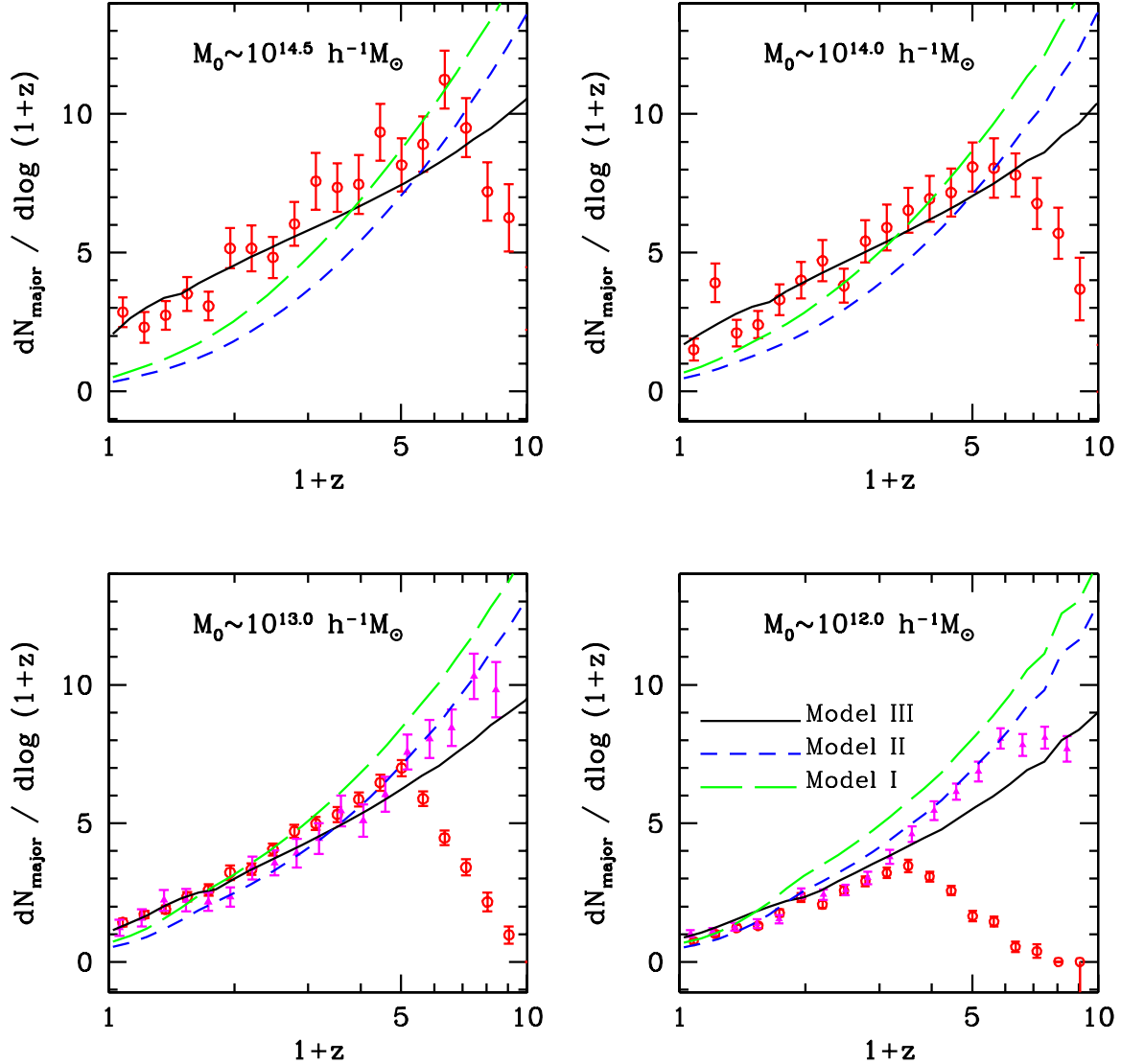
FIG. 5.— The major merger events per unit $\log(1+z)$ as a function of z. The symbols show results obtained from simulations, while the three curves in each panel show the predictions of Models I, II and III. For comparison, results for both the high-resolution (which extends to higher redshift; filled triangles) and low-resolution (open circles) simulations are shown for cases where the the statistic is sufficiently good.

show for comparison. As one can see, the treatment of the unbound halos is able to remove the spurious upturn at the low-mass end. But for sure and to be conservative, the results presented below are all for subhalos containing at least 100 particles.

The long dashed lines in Fig. 4 show the predictions of Model I. This model does not match very well with the simulation results, especially for massive halos at low redshifts. As shown in the upper-right panel of Fig. 4, for massive host halos this model significantly over-predicts the number of accreted low-mass subhalos and under-predicts that of accreted massive subhalos. Such discrepancy has already been noticed and extensively discussed in literature (e.g. Sheth & Tormen 2002; Cole et al. 2008; Parkinson et al. 2008; Neistein et al. 2010). An empirical modification was suggested by Parkinson et al. (2008), which is adopted in our Model II. The results obtained from this model are shown in Fig. 4 as the dashed lines. As one can see, this modification suc-

cessfully suppresses low-mass subhalos, but makes the under-prediction of massive subhalos worse. Finally, let us look at our Model III, the results of which are shown in Fig. 4 as solid curves. Clearly, Model III matches the simulation results much better than either model I or II, especially for massive hosts.

Note that all three models shown have adopted the correction of Eq. (22). If we use model III without this correction, the model underpredicts the abundance of subhalos (as defined using the first definition described in §3.2), especially for low-mass host halos at low redshifts. For completeness, we have also tested model III without the dispersion in halo assembly histories. As expected, not taking this dispersion into account yields conditional subhalo mass functions in poor agreement with the simulation, especially at higher redshifts. Hence, we caution that it is important to properly account for the dispersion in halo assembly histories.
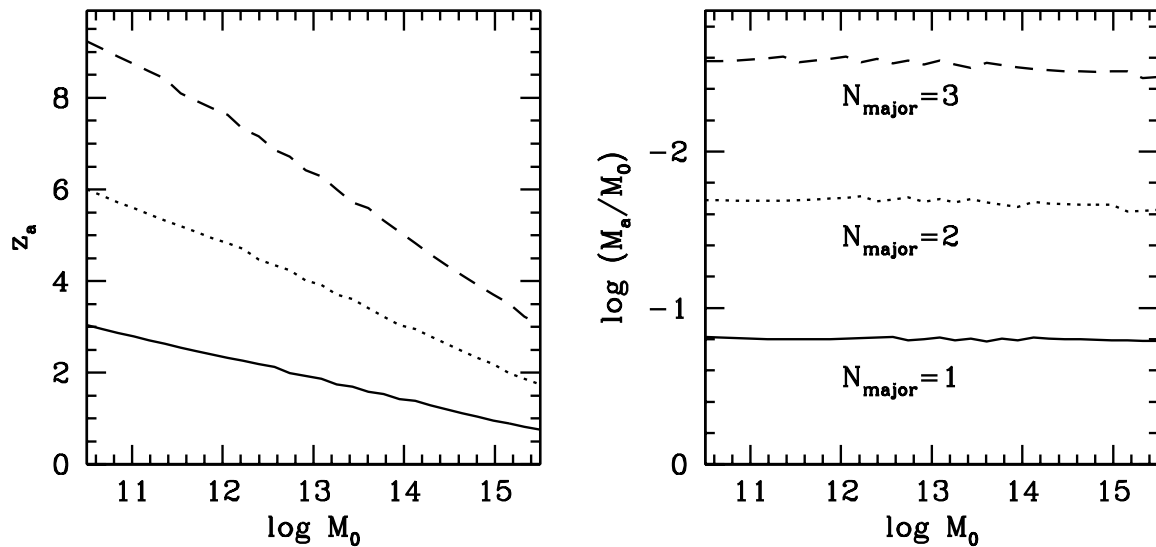
FIG. 6.— The average redshifts below which (left panel) and the average main progenitor to host halo mass ratios above which (right panel) that subhalos have experienced 1st (solid), 2nd (dotted), 3rd last (dashed lines) major merger events, predicted by Model III.

4.2. *Redshift distribution of major mergers*

With the conditional mass functions described above, it is straightforward to calculate the accretion rate of subhalos as a function of host halo mass and redshift. Here we focus on the rates of major mergers where the mass of the accreted subhalo is required to be $m_a \geq M_a/3$. This mean rate in terms of redshift interval can be written as

$$\frac{dN_{\mathrm{major}}}{d\ln(1+z_a)} = \int_{M_a/3}^{M_a} \mathcal{N}_a(s_a, \delta_a | S_0, \delta_0) \frac{dm_a}{m_a} . \quad (23)$$

Note that since the major mergers are defined with respect to individual main branch masses M_a, here we do not include the lognormal scatter (Eq. (21)) in performing the integration. The predictions of Models I, II and III are shown in Fig. 5 as the long dashed, dashed and solid lines, respectively. To check the model predictions we calculate the same quantity directly from the N-body simulations and the results are shown in Fig. 5 as symbols with error bars. For comparison, we show the results obtained from both the $300\,h^{-1}$Mpc and $100\,h^{-1}$Mpc simulation boxes. In the case of the more massive halos (upper two panels), however, we do not show the results from the $100h^{-1}$Mpc simulation box, since these are very noisy due to small number statistics. The $300\,h^{-1}$Mpc box, although having better statistics, has insufficient mass resolution to properly resolve the merger statistics of low mass halos at higher redshifts (as is clearly evident from the lower two panels). Clearly, the results of model III are in very good agreement with the simulation results, and fair much better than either Model I or Model II. In what follows, we focus only on the predictions of Model III.

From the model for the major merger rates in halos of different masses and at different redshifts, we can also predict the characteristic redshift and the characteristic mass associated with the last major merger. By integrating Eq. (23) over redshift from 0 to some z_a, we can obtain the average number of major mergers, N_{major}, expected in this redshift interval. We call the value of z_a

the characteristic redshift, and the main-branch mass at this redshift the characteristic mass of the last N_{major}th major mergers. In Fig. 6 we show the characteristic redshift (left panel) and characteristic mass (right panel) as functions of host-halo mass, for $N_{\mathrm{major}} = 1$, 2 and 3, corresponding to the 1st, 2nd and 3rd last major merger, respectively. Since more massive halos assemble later (see Fig.1), their last major mergers, on average, occur at lower redshifts, as shown clearly in the left-hand panel of Fig. 6 (see similar findings in Li et al. (2007)). Interestingly, the characteristic mass of those last major mergers, in units of the host halo mass, is virtually independent of the host halo mass. This is a manifestation of the fact that all halos (in the mass range explored here) have average merger histories that are self-similar if they are allowed to be stretched or shortened along the time-axis. For example, it is interesting to notice that the average time interval between major mergers is roughly the same as the time during which the main branch mass increases by a constant factor, about $10^{0.8}$, quite independent of the host halo mass.

In a recent paper based on the Millennium simulations, Fakhouri et al. (2010) have come up with a fitting formula which describes the subhalo accretion rates obtained from the simulations. However, since their fitting formula is not based on cosmology-independent quantities, it is only valid for the particular cosmology adopted in the Millennium simulations (see Section 5.1 for more details).

4.3. *Redshift distribution of subhalo accretion*

In Fig. 7 we show our model predictions for the distribution of the accretion redshift for subhalos with $m_a/M_0 = 0.1$ (solid lines), 0.03 (dotted lines) , 0.01 (dashed lines), 0.003 (long dashed lines) and 0.001 (dot-dashed lines), respectively. The results are obtained using Eq. 5 by making some simple coordinate transformations. Results shown in different panels are for host halos of different masses, as indicated. Open circles and filled triangles indicate the results obtained from the $300\,h^{-1}$Mpc and $100\,h^{-1}$Mpc simulations boxes, respec-
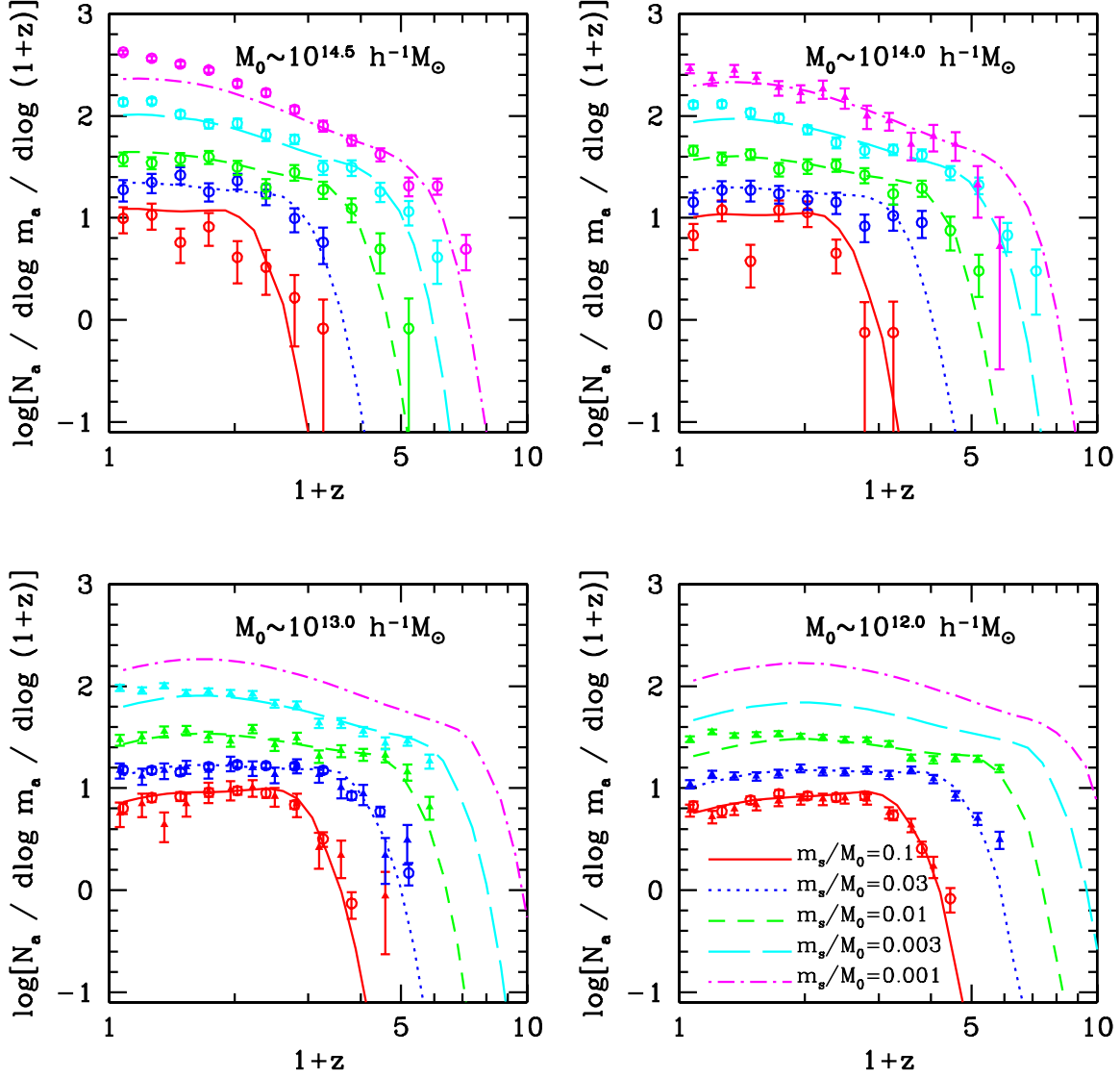
FIG. 7.— Model predictions for the distribution of accretion redshifts for subhalos with $m_a/M_0 = 0.1$ (solid lines), 0.03 (dotted lines), 0.01 (dashed lines), 0.003 (long dashed lines) and 0.001 (dot-dashed lines) respectively. Results are shown for host halos of different masses as indicated in the panels. These results assume a ΛCDM universe and are compared with the results obtained from the $300\,h^{-1}$Mpc box N-body simulations with the same cosmology (open circles). For comparison, results obtained from the $100\,h^{-1}$Mpc box simulations are also shown (as filled triangles) for cases where statistics are sufficiently good.

tively, where the error-bars have been obtained using 200 bootstrap resamples. The various lines show the predictions based on Model III, and overall match the simulation results remarkably well. Note that the accretion rate depends strongly on the mass of the host halo. For the same mass ratio, subhalos in more massive hosts are accreted later, reflecting the hierarchical nature of structure formation in the ΛCDM cosmology.

4.4. Un-evolved subhalo mass functions

Finally, let us look at the un-evolved subhalo mass functions. By integrating Eq. (3) over a given redshift range, we can obtain the un-evolved mass function of the subhalos accreted in that redshift range. In Fig. 8 we show the un-evolved mass functions of subhalos accreted in the redshift ranges [0, 1], [1, 2], [2, 3], [3, 4] and [4, 5], respectively. Results are shown for host halos of different masses, as indicated in each panel. Here

again, symbols indicate the results from our simulation boxes, while lines show the predictions of Model III. Clearly, our model is in excellent agreement with the simulation results at all redshifts and for all host masses. Upon close inspection, it is clear that the un-evolved subhalo mass function for a given redshift range depends on host halo mass, especially at high redshift: in terms of the scaled mass, m_a/M_0, the subhalo mass function at high z is significantly higher for lower-mass host halos. Moreover, the normalization of the un-evolved subhalo mass function at a given redshift for halos of different masses seem to be roughly proportional to the assembly history of the host halos shown in Fig. 1. To test this, we show in Fig. 9 the un-evolved subhalo mass functions for different host halos at the time when the host halos have assembled a fixed fraction of their final masses, i.e. for subhalos accreted in a given range of $\log[\mathcal{M}_a/M_0]$ range. Results are shown for five dif-
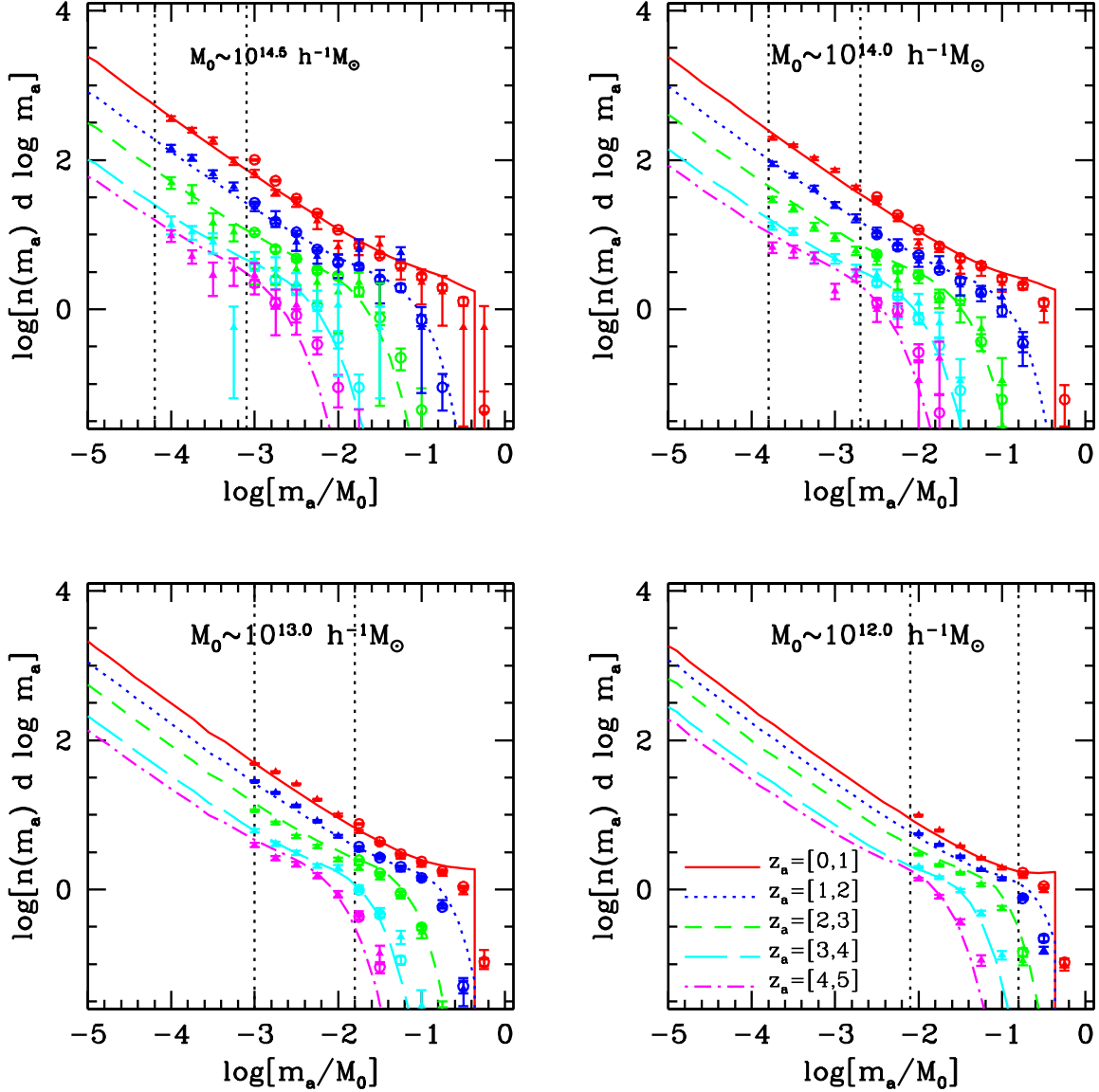
FIG. 8.— The un-evolved mass function of subhalos accreted within the redshift ranges [0, 1] (solid lines), [1, 2] (dotted), [2, 3] (dashed), [3, 4] (long dashed) and [4, 5] (dot-dashed), for host halos of different masses, as indicated in each panel. Here model predictions assuming a ΛCDM cosmology are compared with the the results obtained from the 300 h^{-1}Mpc box N-body simulations of the same cosmology (open circles). For comparison, results obtained from the 100 h^{-1}Mpc box simulation are also shown (as filled triangles) for cases where the statistics are sufficiently good. The vertical lines in each panel correspond to the mass of 100 particles in the two simulations, as in Fig. 4).

ferent ranges of $\log[\mathcal{M}_a/M_0]$: $[-0.5, 0.0]$ (solid lines), $[-1.0, -0.5]$ (dotted), $[-1.5, -1.0]$ (dashed), $[-2.0, -1.5]$ (long dashed), and $[-2.5, -2.0]$ (dot-dashed). For each range of $\log[\mathcal{M}_a/M_0]$ the subhalo mass functions for four host halo masses, $M_0 \sim 10^{14.5}$, $10^{14.0}$, $10^{13.0}$, and $10^{12.0}h^{-1}$M$_\odot$, are plotted with the same line style. Interestingly, the mass function of subhalos accreted in a given range of $\log[\mathcal{M}_a/M_0]$ is almost independent of the host halo mass, demonstrating that the amplitude of of the un-evolved subhalo mass function at a given redshift is directly related to the mass assembly rate of the host halo at that redshift (see also Giocoli 2010).

Integrating Eq. (3) over the *full* redshift range (here for practice we adopt redshift range $z = 0 - 10$) yields the *total* un-evolved subhalo mass function. The results are plotted in the left-hand panel of Fig. 10 for host ha-

los of different masses. Interestingly, although host halos of different masses accrete their subhalos at different redshifts, their total un-evolved subhalo mass functions are extremely similar, both in the simulations (symbols) and in the model (lines). Note, though, that this universality of the un-evolved subhalo mass function, first hinted at in van den Bosch et al. (2005), is only approximate. This is due to the fact that the un-evolved subhalo mass function depends on the *shape* of the perturbation power spectrum around the mass scale in question. For the ΛCDM cosmology considered here, the slope of the power spectrum only changes by a small amount over the mass range $10^{12}\,h^{-1}$M$_\odot \lesssim M_0 \lesssim 10^{15}\,h^{-1}M_\odot$. Indeed, close inspection of the left-hand panel of Fig. 10 reveals small differences between the curves for different host masses.

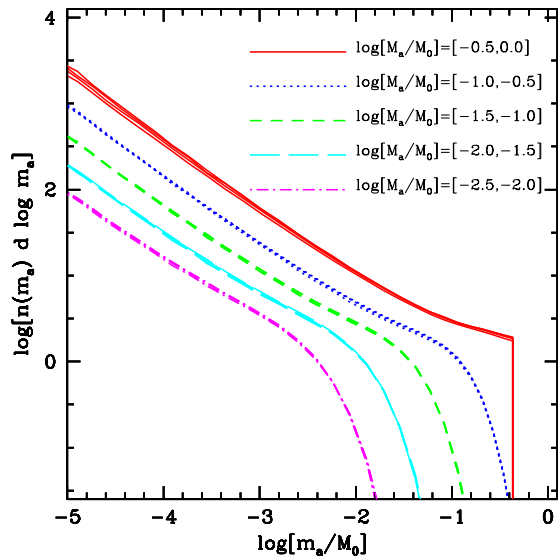FIG. 9.— The un-evolved mass function of subhalos accreted within different $\log[\mathcal{M}_a/M_0]$ ranges [-0.5, 0.0] (solid lines), [-1.0, -0.5] (dotted), [-1.5, -1.0] (dashed), [-2.0, -1.5] (long dashed) and [-2.5, -2.0] (dot-dashed). For each range of $\log[\mathcal{M}_a/M_0]$, results are shown with the same line style for host halos of four different masses: $M_0 \sim 10^{14.5}$, $10^{14.0}$, $10^{13.0}$, and $10^{12.0} h^{-1} \mathrm{M}_\odot$. Note that shown in this way the results for different M_0 are almost indistinguishable.

To further illustrate the dependence of the un-evolved subhalo mass function on the shape of the power spectrum, the right-hand panel of Fig. 10 shows the model predictions for the total un-evolved subhalo mass functions for scale-free models with power spectra with spectral indices $n = 0$ (dashed line), $n = -1$ (long dashed line) and $n = -2$ (dot-dashed line), respectively, together with that for $10^{12} h^{-1} \mathrm{M}_\odot$ host halos in our ΛCDM cosmology (dotted line). The prediction for the $n = -2$ model is very close to that of the ΛCDM model, reflecting the fact that the effective spectral index of the ΛCDM power spectrum is close to -2 over the mass scales in question. The subhalo mass functions for the $n = 0$ and $n = -1$ models are much shallower.

Finally, for comparison, the solid line in the left-hand panel of Fig. 10 shows the fitting formula obtained by Giocoli et al. (2008a) from N-body simulations of the ΛCDM model. This fitting formula agrees well with our model prediction for the ΛCDM model, except at the high mass end where it is slightly lower than our model prediction. Compared to the N-body simulation results, our model prediction agrees with the data slightly better, except perhaps at the very high massive end.

5. DISCUSSION

In this paper we have developed an analytical model for the mass function of CDM subhalos at their time of accretion and for the distribution of their accretion times. This model can be used to predict the un-evolved subhalo mass function, the mass function of subhalos accreted at a given time, the accretion-time distribution of subhalos of a given initial mass, and the frequency of major mergers as a function of time. We have tested our model against results obtained from high-resolution N-body simulations, and found that the model predictions match the simulation results extremely well. In this sec-

tion, we first discuss the universality of our model based on the ingredients used in the construction of the model. We then briefly describe two possible applications of our model.

5.1. The Universality of the Model

The first ingredient of our model is the adopted form for $F(s_a, \delta_a | S_0, \delta_0; M_a)$. As described in Section 3.1, all of our three models, I, II and III, are based on the extended PS theory, which has been shown to work reasonably well for various hierarchical models (e.g. Lacey & Cole 1994; Cole et al. 2008). The modifications made in Models II and III have not been tested for other cosmological models. However, the fact that these models work well for the ΛCDM model over a large redshift range, during which the cosmological parameters change by fairly large amounts, suggests that the modifications should also work for other cosmological models with similar power spectra. Unfortunately, the effective power indices covered by the ΛCDM spectrum are limited, and it is presently unclear whether the modifications will work equally well for models with vastly different power spectra. It will be interesting to test the validity of our model using scale-free models that cover a large range in spectral indices.

The second ingredient of our model is the form of $P(M_a|S_0, \delta_0)$ described in Section 3.2. As tested extensively in Zhao et al. (2009), their model for the median accretion history is universal and works not only for realistic CDM models but also for scale-free models with different spectral indices. Since our tests cover a range of redshifts over which the cosmological parameters change by a large amount, we expect the log-normal form of $P(M_a|S_0, \delta_0)$, and the mass dependence of its dispersion (Eq. [21]), to also apply to other models that have a power-spectrum that is not too different from that of the ΛCDM cosmology considered here. Here again, it will be interesting to test the validity of our model for other power spectra using scale-free models.

Similar arguments also apply to the correction given by Eq. (22). This 'correction' is empirically obtained by Zhao et al. (2009) from various CDM and scale-free models. As discussed in §3.2, using the model with or without this 'correction' corresponds to two different definitions of the un-evolved subhalo population, and only has a non-negligible impact when it comes to subhalos accreted at low redshifts in low-mass host halos.

To summarize, we believe that our model holds for any variant of the ΛCDM model. In particular, it should work accurately for any cosmological model whose parameters are in agreement with current observational constraints from the cosmic microwave background, supernovae Ia, and galaxy redshift surveys.

5.2. Applications

Our model has a number of applications. Here we focus on two of them: (i) the evolution of subhalos as they orbit within their hosts, and (ii) the construction of a self-consistent model to link galaxies and dark matter halos across cosmic time.

The model described here applies to subhalos at accretion, i.e. the un-evolved population of subhalos. However, as a small halo merges with and orbits in
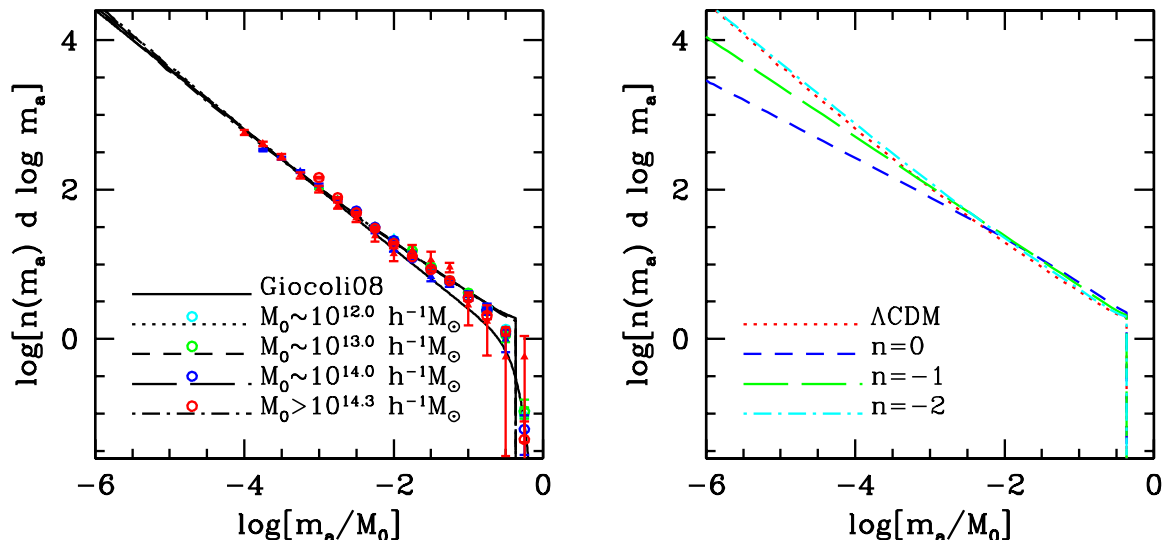
FIG. 10.— Left panel: the un-evolved subhalo mass distribution as a function of m_a/M_0 for host halos of different final masses at $z = 0$. Here model predictions (lines) are compared with the results obtained from both the $300\ h^{-1}$Mpc box (open circles) and $100\ h^{-1}$Mpc box (filled triangles) N-body simulations of the same cosmology. For comparison, we also include in the figure the fitting formula obtained by Giocoli et al. (2008a) as the solid line. Right panel: The predicted un-evolved subhalo mass functions for scale-free models with $n = 0$, -1 and -2. For comparison, we also include in the figure the model prediction for the ΛCDM model considered in this paper.

a larger halo, it is subjected to tidal forces from the host, causing it to lose mass, and to dynamical friction, which causes it to lose energy and angular momentum to the dark matter particles of the host. Thus, dynamical evolution after accretion can change the properties of the subhalo population. A great deal of work has been done to understand the properties of the 'evolved' subhalo population, using either numerical simulations (e.g. Klypin et al. 1999; Moore et al. 1999; Springel et al. 2001b; Diemand et al. 2004, 2007; Gao et al. 2004; Kang et al. 2005; Springel et al. 2008; Wetzel & White 2010), or merger trees constructed from the extended PS formalism (e.g. Taylor & Babul 2001, 2004, 2005; van den Bosch et al. 2005; Zentner et al. 2005; Giocoli et al. 2008a; Gan et al. 2010).

After accretion, whether a subhalo can survive as a self-bound entity depends on its mass (relative to that of its host), its density profile (which is related to its accretion redshift), and its orbit. The model presented here provides information about the first two parts. Thus, combined with information about the initial orbits of accreted subhalos (e.g. van den Bosch et al. 1999; Khochfar & Burkert 2006; Ludlow et al. 2009; Valluri et al. 2010; Wetzel 2011) and about how dynamical friction and tidal stripping operate on subhalos (e.g. Jiang et al. 2008; Boylan-Kolchin et al. 2008), our model can be used to construct models for the evolved subhalo population, such as their mass function, their distribution in host halos, and their correlation with host halo properties. We will come back to such modeling in a future paper.

The last decade has seen much effort in using halo occupation statistics to describe the galaxy-dark matter connection in an attempt to understand the galaxy luminosity function, galaxy clustering, galaxy-galaxy lensing, and the kinematics of satellite galaxies (e.g. Mo, Mao & White 1999; Berlind & Weinberg 2002; Yang et al. 2003; van den Bosch et al. 2003; Zheng et al. 2005; Tinker et al. 2005; Cooray 2005,

2006; Cooray & Ouchi 2006; Vale & Ostriker 2004, 2006; van den Bosch et al. 2007; Yang et al. 2009; Cacciato et al. 2009; More et al. 2009; Moster et al. 2010). Several of these studies have tried to make a direct link between the halo occupation statistics of galaxies and of dark matter subhalos, using abundance matching techniques to link satellite galaxies to subhalos (e.g. Kravtsov et al. 2004; Conroy et al. 2006, 2007; Conroy & Wechsler 2009; Behroozi et al. 2010; Wang & Jing 2010; Wetzel & White 2010; Neistein et al. 2011; Avila-Reese & Firmani 2011). These investigations typically rely on the un-evolved subhalo mass function, but do not account for the possibility that different subhalos are accreted at different times and that the halo mass - galaxy mass relation may be redshift-dependent. In order to construct a self-consistent model based on abundance matching, one needs not only the (un-evolved) subhalo mass function, but also the distribution of accretion times. This is exactly what our model can provide. In a forthcoming paper (Yang et al. 2011), we will construct such a self-consistent model to characterize how the galaxy-dark matter connection evolves over time.

ACKNOWLEDGEMENTS

REFERENCES

Angulo, R. E., Lacey, C. G., Baugh, C. M., & Frenk, C. S. 2009, MNRAS, 399, 983
Avila-Reese, V., Firmani, C., & Hernández, X. 1998, ApJ, 505, 37
Avila-Reese, V., & Firmani C. 2011, preprint (arXiv:1103.4329)
Behroozi, P. S., Conroy, C., & Wechsler, R. H. 2010, ApJ, 717, 379
Berlind A. A., Weinberg D. H., 2002, ApJ, 575, 587
Berlind A. A. 2003, ApJ, 593, 1
Benson, A. J., Frenk, C. S., Baugh, C. M., Cole, S., & Lacey, C. G. 2001, MNRAS, 327, 1041
Bond J. R., Cole S., Efstathiou G., Kaiser N., 1991, ApJ, 379, 440
Bower, R. G. 1991, MNRAS, 248, 332
Boylan-Kolchin, M., Ma, C.-P., & Quataert, E. 2008, MNRAS, 383, 93
Cacciato, M., van den Bosch, F. C., More, S., Li, R., Mo, H. J., & Yang, X. 2009, MNRAS, 394, 929
Cole, S., Helly, J., Frenk, C. S., & Parkinson, H. 2008, MNRAS, 383, 546
Cole, S., Lacey, C. G., Baugh, C. M., & Frenk, C. S. 2000, MNRAS, 319, 168
Conroy, C., Wechsler, R. H., & Kravtsov, A. V. 2006, ApJ, 647, 201
Conroy, C., Wechsler, R. H., & Kravtsov, A. V. 2007, ApJ, 668, 826
Conroy, C., & Wechsler, R. H. 2009, ApJ, 696, 620
Cooray, A. 2005, MNRAS, 364, 303
Cooray, A. 2006, MNRAS, 365, 842
Cooray, A., & Ouchi, M. 2006, MNRAS, 369, 1869
Davis M., Efstathiou G., Frenk C.S., White S.D.M., 1985, ApJ, 292, 371
De Lucia G., Kauffmann G., Springel V., White, S. D. M., Lanzoni B., Stoehr F., Tormen G., & Yoshida N. 2004, MNRAS, 348, 333
Diemand, J., Moore, B., & Stadel, J. 2004, MNRAS, 352, 535
Diemand, J., Kuhlen, M., & Madau, P. 2007, ApJ, 667, 859
Dunkley, J., et al. 2009, ApJS, 180, 306
Fakhouri O., Ma C. P., 2008, MNRAS, 386, 577
Fakhouri, O., Ma, C.-P., & Boylan-Kolchin, M. 2010, MNRAS, 406, 2267
Gan, J., Kang, X., van den Bosch, F. C., & Hou, J. 2010, MNRAS, 408, 2201
Gao L., White S. D. M., Jenkins A., Stoehr F., Springel V., 2004, MNRAS, 355, 819
Giocoli C., Tormen G., van den Bosch F. C., 2008a, MNRAS, 386, 2135
Giocoli C., Pieri L., Tormen G., MNRAS, 2008b, 387, 689
Giocoli, C. 2010, American Institute of Physics Conference Series, 1241, 892
Jiang, C. Y., Jing, Y. P., Faltenbacher, A., Lin, W. P., & Li, C. 2008, ApJ, 675, 1095
Kang, X., Jing, Y. P., Mo, H. J., Börner, G. 2005, ApJ, 631, 21
Khochfar, S., & Burkert, A. 2006, A&A, 445, 403
Klypin, A., Gottlöber, S., Kravtsov, A. V., & Khokhlov, A. M. 1999, ApJ, 516, 530
Kravtsov, A., Berlind, A.A., Wechsler, R.H., Klypin, A., Gottlöber, S., Allgood, B., & Primack, J.R. 2004, ApJ, 609, 35
Lacey C., Cole S., 1993, MNRAS, 262, 627
Lacey, C., & Cole, S. 1994, MNRAS, 271, 676
Li, R., Mo, H. J., Fan, Z., Cacciato, M., van den Bosch, F. C., Yang, X., & More, S. 2009, MNRAS, 394, 1016
Li Y., Mo H. J., 2009, preprint (arXiv:0908.0301)
Li Y., Mo H. J., van den Bosch F. C., Lin W. P., 2007, MNRAS, 379, 689

Ludlow, A. D., Navarro, J. F., Springel, V., Jenkins, A., Frenk, C. S., & Helmi, A. 2009, ApJ, 692, 931
Mo H. J., Mao S., White S. D. M., 1999, MNRAS, 304, 175
Mo H. J., van den Bosch F. C., White S. D. M., 2010, Galaxy Formation and Evolution, Cambridge University Press
Moore, B., Ghigna, S., Governato, F., Lake, G., Quinn, T., Stadel, J., & Tozzi, P. 1999, ApJ, 524, L19
More, S., van den Bosch, F. C., Cacciato, M., Mo, H. J., Yang, X., & Li, R. 2009, MNRAS, 392, 801
Moster, B. P., Somerville, R. S., Maulbetsch, C., van den Bosch, F. C., Macciò, A. V., Naab, T., & Oser, L. 2010, ApJ, 710, 903
Neistein, E., & Dekel, A. 2008, MNRAS, 383, 615
Neistein, E., Macciò, A. V., & Dekel, A. 2010, MNRAS, 403, 984
Neistein, E., Li, C., Khochfar, S., Weinmann, S. M., Shankar, F., & Boylan-Kolchin, M. 2011, preprint (arXiv:1103.3272)
Parkinson, H., Cole, S., & Helly, J. 2008, MNRAS, 383, 557
Porciani, C., Dekel, A., & Hoffman, Y. 2002, MNRAS, 332, 325
Press, W. H., Schechter, P. 1974, ApJ, 187, 425
Sheth, R. K., & Lemson, G. 1999, MNRAS, 305, 946
Sheth R. K., & Tormen G. 1999, MNRAS, 308, 119
Sheth R. K., Mo H. J., & Tormen G. 2001, MNRAS, 323, 1
Sheth, R. K., & Tormen, G. 2002, MNRAS, 329, 61
Sheth R. K., 2003, MNRAS, 345, 1200
Sheth, R. K., & Tormen, G. 2004, MNRAS, 349, 1464
Somerville, R. S., & Kolatt, T. S. 1999, MNRAS, 305, 1
Springel V., White S. D. M., Tormen G., Kauffmann G., 2001, MNRAS, 328, 726
Springel, V., Yoshida, N., & White, S. D. M. 2001, NewA, 6, 79
Springel V. et al., 2005, Nat., 435, 639
Springel, V., et al. 2008, MNRAS, 391, 1685
Taylor, J. E., & Babul, A. 2001, ApJ, 559, 716
Taylor, J. E., & Babul, A. 2004, MNRAS, 348, 811
Taylor, J. E., & Babul, A. 2005, MNRAS, 364, 515
Tinker J. L., Weinberg D. H., Zheng Z., Zehavi I., ApJ, 2005, 631, 41
Vale, A., & Ostriker, J. P. 2004, MNRAS, 353, 189
Vale, A., & Ostriker, J. P. 2006, MNRAS, 371, 1173
Valluri, M., Debattista, V. P., Quinn, T., & Moore, B. 2010, MNRAS, 403, 525
van den Bosch, F. C., Lewis, G. F., Lake, G., & Stadel, J. 1999, ApJ, 515, 50
van den Bosch, F. C. 2002, MNRAS, 331, 98
van den Bosch, F. C., Yang, X., & Mo, H. J. 2003, MNRAS, 340, 771
van den Bosch F. C., Tormen G., Giocoli C., 2005, MNRAS, 359, 1029
van den Bosch et al., 2007, MNRAS, 376, 841
Wang, L., & Jing, Y. P. 2010, MNRAS, 402, 1796
Wechsler R. H., Bullock J. S., Primack J. R., Kravtsov A. V., & Dekel A. 2002, ApJ, 568, 52
Wetzel, A. R., Cohn, J. D., & White, M. 2009, MNRAS, 395, 1376
Wetzel, A. R., & White, M. 2010, MNRAS, 403, 1072
Wetzel, A. R. 2011, MNRAS, 412, 49
Yang X., Mo H. J., van den Bosch F. C., 2003, MNRAS, 339, 1057
Yang X., Mo H. J., van den Bosch F. C., 2009, ApJ, 693, 830
Yang X., Mo H. J., van den Bosch F. C., Han J., 2011, in preparation
Zentner, A. R., Berlind A. A., Bullock, J. S., Kravtsov, A. V., & Wechsler, R. H. 2005, ApJ, 624, 505
Zhao, D. H., Jing, Y. P., Mo, H. J., & Boerner, G. 2009, ApJ, 707, 354
Zheng Z. et al., 2005, ApJ, 633, 791
Zheng, Z., Coil, A. L., & Zehavi, I. 2007, ApJ, 667, 760